Investigating the Perovskite Ag1-3xLaxNbO3 as a High-Rate Negative Electrode for Li-Ion Batteries

Etienne Le Calvez, Julio César Espinosa-Angeles, Grace Whang, Nicolas Dupré, Bruce Dunn, Olivier Crosnier, Thierry Brousse

frontiers | Frontiers in Chemistry

ORIGINAL RESEARCH
published: 13 April 2022
doi: 10.3389/fchem.2022.873783

Investigating the Perovskite $Ag_{1-3x}La_xNbO_3$ as a High-Rate Negative Electrode for Li-Ion Batteries

*Etienne Le Calvez[1,2], Julio César Espinosa-Angeles[1,2], Grace J. Whang[3], Nicolas Dupré[1], Bruce S. Dunn[3], Olivier Crosnier[1,2] and Thierry Brousse[1,2]**

[1]Nantes Université, CNRS, Institut des Matériaux de Nantes Jean Rouxel, IMN, Nantes, France, [2]Réseau sur le Stockage Electrochimique de l'Energie (RS2E), CNRS FR 3459, Amiens Cedex, France, [3]Department of Materials Science and Engineering, University of California, Los Angeles, Los Angeles, CA, United States

The broader development of the electric car for tomorrow's mobility requires the emergence of new fast-charging negative electrode materials to replace graphite in Li-ion batteries. In this area, the design of new compounds using innovative approaches could be the key to discovering new negative electrode materials that allow for faster charging and discharging processes. Here, we present a partially substituted $AgNbO_3$ perovskite material by introducing lanthanum in the A-site. By creating two vacancies for every lanthanum introduced in the structure, the resulting general formula becomes $Ag_{1-3x}La_x\square_{2x}NbO_3$ (with $x \leq 0.20$ and where $\square$ is a A-site vacancy), allowing the insertion of lithium ions. The highly substituted $Ag_{0.40}La_{0.20}\square_{0.40}NbO_3$ oxide shows a specific capacity of 40 $mAh.g^{-1}$ at a low sweep rate (0.1 $mV\,s^{-1}$). Interestingly, $Ag_{0.70}La_{0.10}\square_{0.20}NbO_3$ retains 64% of its capacity at a very high sweep rate (50 $mV\,s^{-1}$) and about 95% after 800 cycles. *Ex situ* ^{7}Li MAS NMR experiments confirmed the insertion of lithium ions in these materials. A kinetic analysis of $Ag_{1-3x}La_x\square_{2x}NbO_3$ underlines the ability to store charge without solid-state ion-diffusion limitations. Furthermore, *in situ* XRD indicates no structural modification of the compound when accommodating lithium ions, which can be considered as zero-strain material. This finding explains the interesting capacity retention observed after 800 cycles. This paper thus demonstrates an alternative approach to traditional insertion materials and identifies a different way to explore not-so common electrode materials for fast energy storage application.

Keywords: silver niobate, lithium-ion battery, high rate anode material, fast charging, innovative oxide

OPEN ACCESS

Edited by:
Yohan Dall'Agnese, University College London, United Kingdom

Reviewed by:
Martin Wilkening, Graz University of Technology, Austria
Xiao-Dong Zhu, Qingdao University of Science and Technology, China

****Correspondence:***
Thierry Brousse
thierry.brousse@univ-nantes.fr

Specialty section:
This article was submitted to Electrochemistry, a section of the journal Frontiers in Chemistry

Received: *11 February 2022*
Accepted: *18 March 2022*
Published: *13 April 2022*

Citation:
Le Calvez E, Espinosa-Angeles JC, Whang GJ, Dupré N, Dunn BS, Crosnier O and Brousse T (2022) Investigating the Perovskite $Ag_{1-3x}La_xNbO_3$ as a High-Rate Negative Electrode for Li-Ion Batteries. Front. Chem. 10:873783. doi: 10.3389/fchem.2022.873783

INTRODUCTION

To eliminate our dependence on carbon-based energy production, specifically in the field of mobility, it is essential to develop energy storage devices able to store the intermittent energy harvested by renewable energy sources (Armand and Tarascon 2008). A key to the deployment of electric vehicles is the ability of batteries to charge quickly while ensuring long cycle life, and optimized safety (Burnham et al., 2017; Li et al., 2020). The current use of graphite as a negative electrode only partially satisfies these needs (Choi et al., 2020). In fast-charging batteries, graphite enables the insertion of lithium at an average potential close to that of Li^+/Li (0.1 V vs. Li^+/Li), which can lead to the formation of lithium plating followed by dendrite growth, resulting in possible short circuits and thermal runaway. Moreover, the specific capacity of graphite is drastically reduced at high current

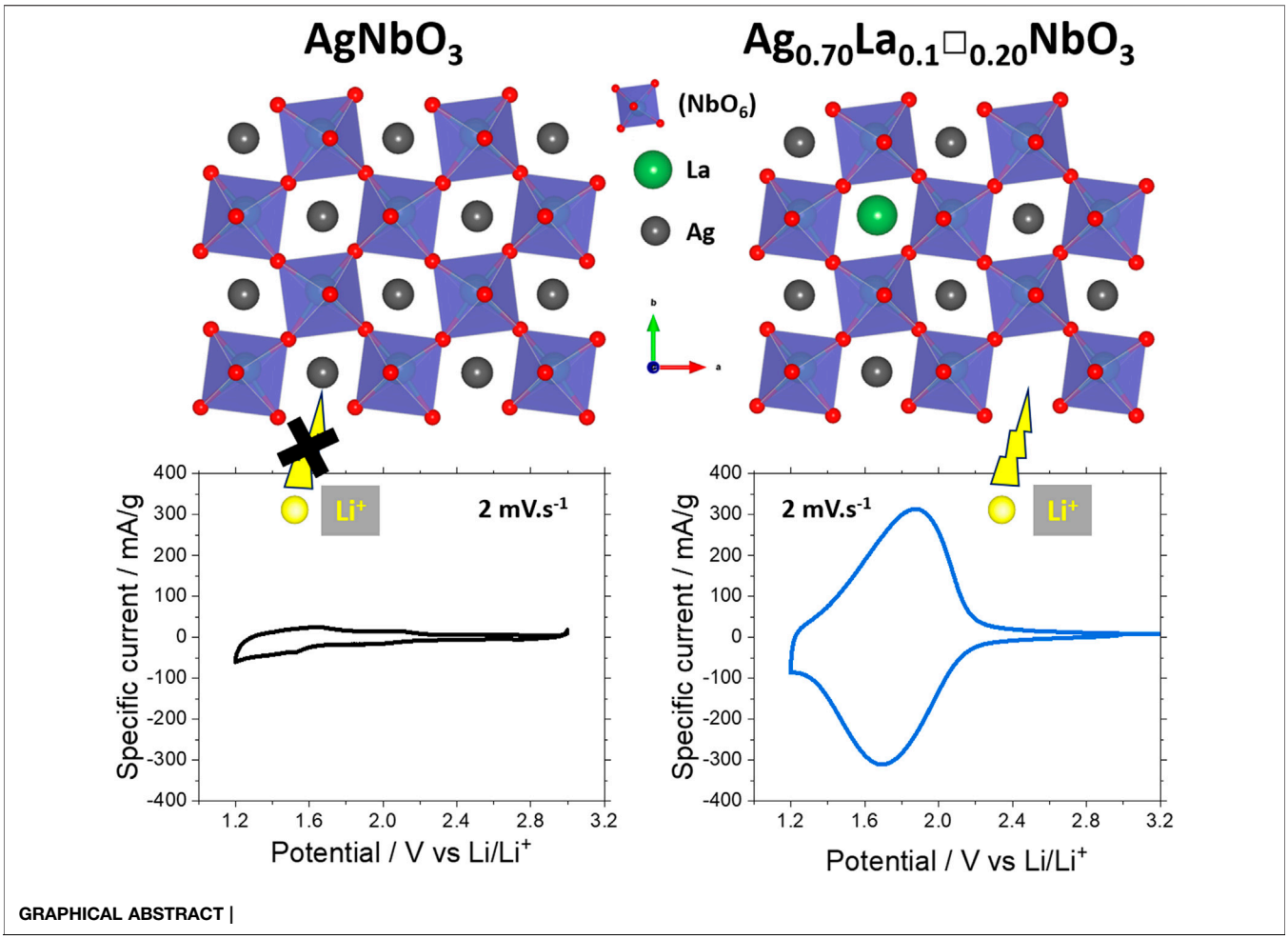

GRAPHICAL ABSTRACT |

densities due to kinetic limitations on ion mobility between graphene layers (Sivakkumar et al., 2010).

For these reasons, alternative negative electrode materials have attracted increased attention over the past decade One of the best known negative electrode materials for high-rate applications is $Li_4Ti_5O_{12}$ (LTO) (Prakash et al., 2010; Song et al., 2014; Thackeray and Amine 2021). Crystallizing in a spinel structure, this zero strain material offers an alternative route towards designing fast charging batteries with a relatively high specific capacity. Moreover, new approaches have been proposed to offer more options for the replacement of graphite electrode. Among others, shear-structure materials including $TiNb_2O_7$ (Griffith et al., 2019) or $Nb_{16}W_{18}O_{93}$ (Griffith et al., 2018) offer relatively large capacity values at high rate between 1V and 3V vs. Li^+/Li. Low volume changes upon lithium insertion and an operating potential that avoids the formation of lithium-consuming solid electrolyte interphase (SEI) are the main advantages offered by these materials. In addition, a new approach has recently been proposed to transform a material traditionally used as an ionic conductor into a material for high-rate Na-ion batteries. Partial substitution of Al by Fe in ß"-Al_2O_3 offers both ionic and electronic conduction, allowing fast and reversible Na^+ intercalation (Butts et al., 2021). This material displays cyclic voltammogram with broad peaks attributed to a surface-controlled charge storage mechanism. Similar approaches are needed to unravel different fast charging materials and their associated mechanisms.

In this work, we propose an alternative way to produce materials that can insert alkali cations with minor diffusion limitation, thus allowing high current density operation. More precisely, the A-site of $AgNbO_3$ perovskite synthesized by sol-gel process has been partially substituted by lanthanum (La^{3+}), allowing the creation of vacancies in this crystallographic site. Insertion of Li ions is observed in every substituted $Ag_{1-3x}La_x\square_{2x}NbO_3$ compound (with $x > 0$), thus leading to experimental specific capacities close to the theoretical values. Calculation of *b*-value shows a non-diffusion-controlled mechanism and *in situ* XRD shows negligible volume expansion (zero strain electrode) during the insertion/deinsertion mechanism for this new family of materials, therefore explaining the cycling stability of $Ag_{1-3x}La_x\square_{2x}NbO_3$.

EXPERIMENTAL SECTION

Synthesis of $Ag_{1-3x}La_x\square_{2x}NbO_3$

$Ag_{1-3x}La_x\square_{2x}NbO_3$ powders were synthesized by a sol-gel route (SG) based on a previous report (Wu et al., 2013). Briefly, a

stoichiometric mixture of $NbCl_5$ (99%, Sigma Aldrich), $La(NO_3)_3$ (99.9%, Alfa Aesar), $AgNO_3$ (99.9%, Alfa Aesar), and citric acid in excess (99+%, Alfa Aesar) was dissolved in 30% (w/w) H_2O_2 in H_2O (Sigma Aldrich). Upon complete dissolution of the species, the solution turned to a dark yellow color. At this point, the solution was heated at 120°C until the formation of a dark brown gel. The latter was heated to 300°C overnight to remove organic moieties and dehydrate the gel. The resulting powder is ground in an agate mortar and then annealed at 650°C for 6 h in an alumina crucible to crystallize the material. Depending on the degree of substitution, the resulting powder ranges from dark grey for $AgNbO_3$ to whitish powder in the case of $Ag_{0.40}La_{0.20}\square_{0.40}NbO_3$.

Characterization

Powder X-Ray Diffraction

X-ray diffraction (XRD) patterns were collected using a PANalytical X'Pert Pro diffractometer (Malvern Panalytical, Almelo, Netherlands). An X'Celerator detector with Cu-Kα1-Kα2 (λ = 1.54060, 1.54439 Å) radiation was used with acceleration voltage and current of 40 kV and 40 mA, respectively. With a step scan of 0.0167°, diffraction patterns have been collected between 20° and 80° (2θ). Using pseudo-Voigt functions, Le Bail refinement was performed using FullProf Suite. Preliminary lattice parameter values have been taken from the literature (Sciau et al., 2004). For *in situ* XRD measurements, patterns were collected using a homemade "Leriche-like" cell (Leriche et al., 2010). During charge-discharge experiment, a current of 0.005 A g^{-1} was applied for 20 min and stopped during 30 min for XRD pattern acquisition.

Electron Microscopy and Energy Dispersive X-Ray Analyses

The morphology and particle size were studied with a transmission electron microscope ThermoFisher S/TEM Themis G3 at 300 kV (Breda) point to point resolution: 0.18 nm. SEM micrographs were obtained at 20 kV using a Zeiss MERLIN Instrument using in-Lens annular detector. Samples were prepared by dispersing a small fraction of the powder on a piece of conducting carbon tape. EDX was collected at 8.0 mm working distance using an X-Max 50 mm^2 OXFORD Instruments detector. The measurements were performed on at least two samples per synthesis and for each sample at least 10 acquisitions were performed. The atomic percentage of each cation was determined with an accuracy of ±5%.

BET Measurement

The specific surface area of the powders was determined using the BET method (Brunauer-Emmett-Teller) from the 77 K nitrogen adsorption curves with a Quantachrome Nova 4200e equipment (Anton Paar).

Electrochemistry

Self-supported electrodes were fabricated by mixing, in a small amount of ethanol, 75% w/w $Ag_{1-3x}La_x\square_{2x}NbO_3$, 15% w/w of conductive carbon (Carbon Black by Superior Graphite, Chicago, IL, United States) to increase electronic conductivity and 10% w/w poly (1,1,2,2-tetrafluoroethylene) dissolved in water (PTFE, Sigma Aldrich) to form a homogeneous paste. This mixture was homogenized in a mortar and then cold-rolled until electrodes with a mass loading of about 5–10 mg cm^{-2} were obtained. This level of loading enables reliable gravimetric values to be reported (Gogotsi and Simon 2011). Electrochemical measurements were performed using Swagelok cells. The positive electrode and metallic lithium (99.9%, Aldrich) were separated using a glass fiber membrane (70 mm, 10 mm diameter, GF/D Whatman) soaked with 1M $LiPF_6$ dissolved in 1:1 %wt. EC/DMC (Solvionic, France, battery grade purity). The Swageloks were assembled in a glove box containing less than 0.1 ppm of O_2 and H_2O. A VMP3 potentiostat (from Biologic run under ECLab software version V11.36, Seyssinet-Pariset, France) was used for electrochemical measurements.

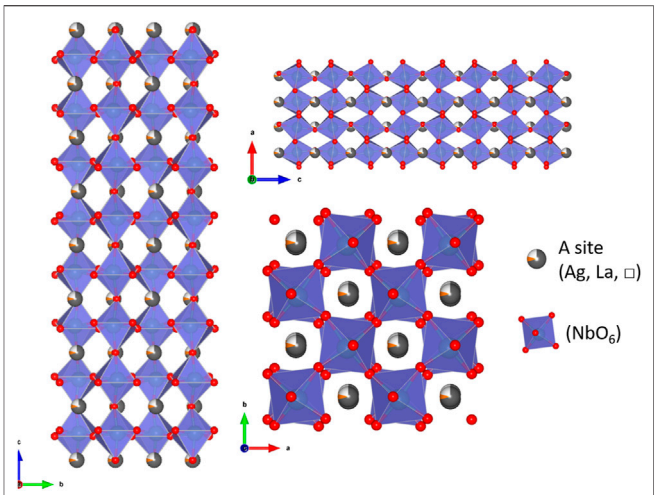

FIGURE 1 | (A-B-C) respectively a, b, and c axis view of $Ag_{0.70}La_{0.10}\square_{0.20}NbO_3$.

Ex situ MAS NMR

For MAS NMR analysis, free-standing electrodes with about 5–10 mg cm^{-2} were polarized for 10 h at different states of charge after performing a cyclic voltammogram (CV) at 0.1 mV s^{-1}. After disassembling the Swageloks in a glove box, electrodes were cleaned with a few drops of DMC and then dried overnight under *vacuum* in a Büchi oven at 60°C. Then, the electrolyte-free electrode was placed in a 2.5 mm-diameter zirconia rotor for MAS NMR experiments. ^{7}Li MAS NMR spectra were acquired on a Bruker Avance 200 spectrometer (B0 = 4.7 T, Larmor frequencies ν_0 (^{7}Li = 77.78 MHz) at RT. A Bruker MAS probe with a cylindrical 2.5 mm (o.d) zirconia rotor spun at a frequency of 30 kHz was used. Spectra were obtained by applying a single pulse sequence, and a recycle delay (D1) of 3s ensured the acquisition of quantitative spectra. ^{7}Li integrated intensities were determined by using spectral simulation (DMFit Software) (Massiot et al., 2002). The resulting integrated intensities were normalized with respect to the mass of the sample contained in the NMR rotor, the number of scans, and the receiver gain. Due to low amount of lithiated active material used for the analyses, it was not possible to rely on ^{6}Li MAS NMR to characterize local structural features.

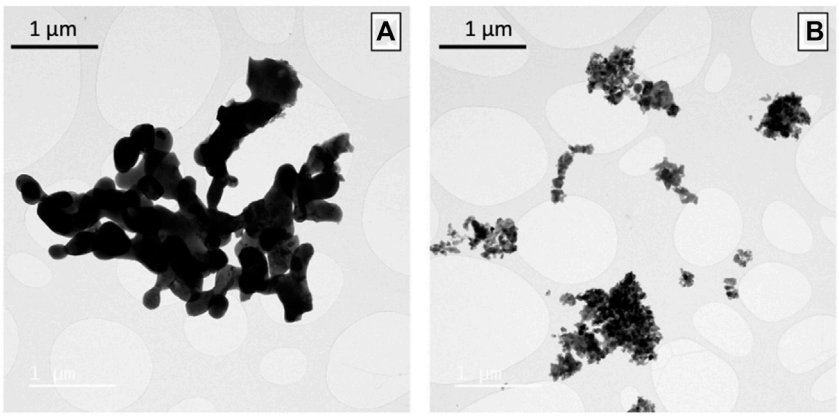

FIGURE 2 | TEM images of **(A)** $AgNbO_3$ and **(B)** $Ag_{0.70}La_{0.10}\square_{0.20}NbO_3$ after annealing at 650°C showing the difference in particles size between unsubstituted and substituted oxides.

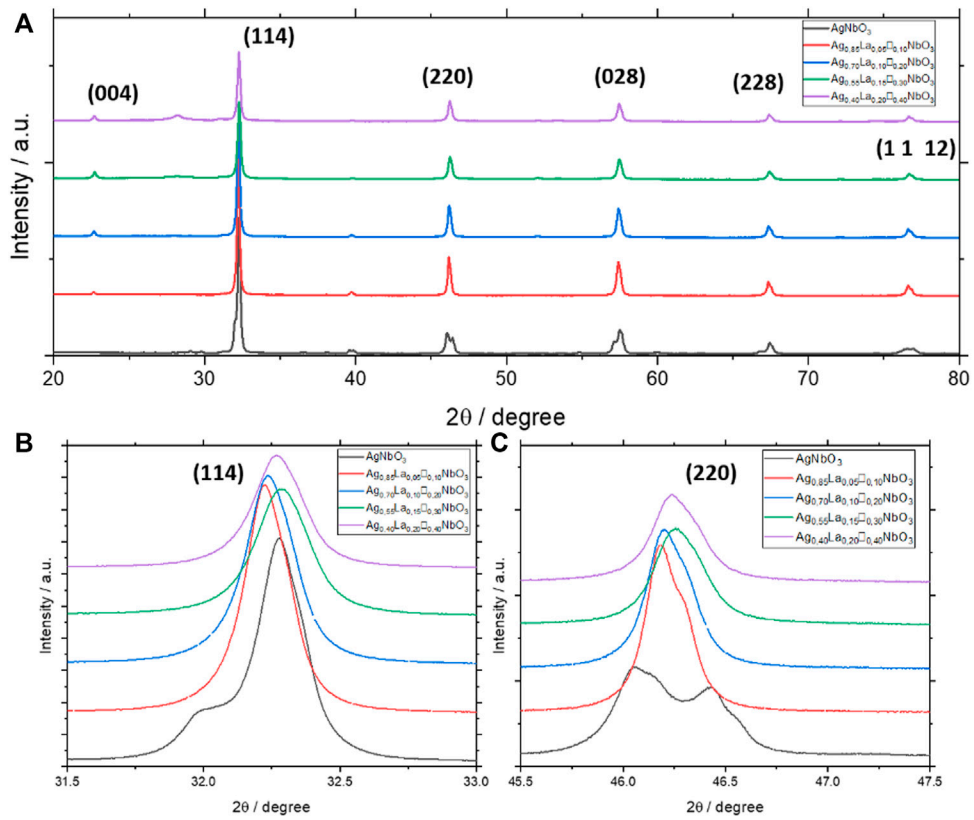

FIGURE 3 | (A–C) XRD patterns of $Ag_{1-3x}La_x\square_{2x}NbO_3$ for different value of x.

RESULTS AND DISCUSSIONS

At room temperature, $AgNbO_3$ crystallizes in an orthorhombic perovskite structure (space group Pbcm) with distorted $[BO_6]$ octahedra, similar to most perovskites (Sciau et al., 2004). Historically, $AgNbO_3$ has been studied in material science as antiferroelectric material for energy storage applications. Substitutions in this lead-free material have been widely examined to stabilize the antiferroelectric phase and increase the power density. Various studies have explored the substitution of Ag^+ in $AgNbO_3$ by Li^+ (Farid et al., 2019), Na^+ (Takeda et al., 2003), and multivalent cations (Li et al., 2009; Juang et al., 2016; Gao et al., 2020) (Sr^{2+}, La^{3+}, Sm^{3+}, etc.) to create A-site vacancies. All the substitutions by multivalent cations show an increase in

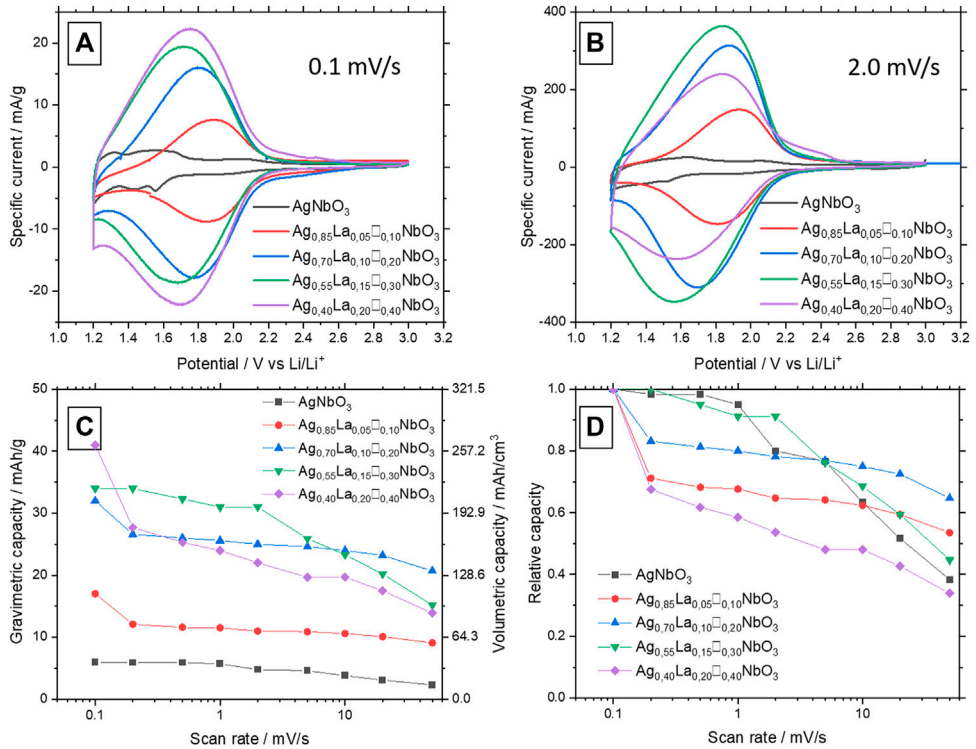

FIGURE 4 | (A) CV at 0.1 mV s^{-1} between 1.2 and 3 V of $Ag_{1-3x}La_x{}^{\square}{}_{2x}NbO_3$ for different value of x. **(B)** CV at 2.0 mV s^{-1} between 1.2 and 3 V of $Ag_{1-3x}La_x{}^{\square}{}_{2x}NbO_3$ for different value of x. **(C)** Specific capacity of $Ag_{1-3x}La_x{}^{\square}{}_{2x}NbO_3$ for different value of x in function of the scan rate. **(D)** Relative capacity of $Ag_{1-3x}La_x{}^{\square}{}_{2x}NbO_3$ for different value of x in function of the scan rate.

the symmetry of the material until the presence of impurities at a high degree of substitution (Juang et al., 2016; Gao et al., 2019; Gao et al., 2020). In order to investigate the possible Li-ion insertion into A site vacancies of this perovskite, we synthesized La-doped $AgNbO_3$ with different substitution ratios from x = 0 to x = 0.20. In a perovskite lattice, the coordination number of the A-site is 12, and 6 for the B-site. The ionic radius of silver is 1.54 Å, whereas that of niobium is 0.64 Å (Shannon and Prewitt 1969; Shannon 1976). Since the ionic radius of La for a coordination number of 12 is 1.36 Å, the silver-to-lanthanum substitution should be effective in the A site of the perovskite $Ag_{1-3x}La_x{}^{\square}{}_{2x}NbO_3$, where □ depicts a cation, vacancy in the A site of the perovskite, following reaction **Eq. 1**:

$$La_2O_3 \rightarrow 2La^{\cdot\cdot}_{Ag} + 3O^x_o + 4V'_{Ag} \quad (1)$$

Here, we will name the samples $Ag_{0.85}La_{0.05}{}^{\square}{}_{0.10}NbO_3$, $Ag_{0.70}La_{0.10}{}^{\square}{}_{0.20}NbO_3$, $Ag_{0.55}La_{0.15}{}^{\square}{}_{0.30}NbO_3$ and $Ag_{0.40}La_{0.20}{}^{\square}{}_{0.40}NbO_3$, respectively for x = 0.05, x = 0.10, x = 0.15 and x = 0.20. **Figure 1** represents the crystallographic arrangement of $Ag_{0.70}La_{0.10}{}^{\square}{}_{0.20}NbO_3$ which shows both distortion of [NbO_6] octahedra and the partial substitution of Ag by La in A-site with the corresponding vacancies.

The synthesis of $Ag_{1-3x}La_x{}^{\square}{}_{2x}NbO_3$ by a ceramic route was difficult to achieve. One reason is the reduction of Ag_2O to metallic Ag for a temperature higher than 150°C (Chun et al., 2009; Shin et al., 2013). A second reason is the thermodynamic competition between $AgNbO_3$ and $Ag_2Nb_4O_{11}$ does not allow one to easily obtain a phase pure material, even by adding an excess of Ag_2O (Valant et al., 2007). For this reason, the different stoichiometries of $AgNbO_3$ were synthesized by a sol-gel (SG) process which has been demonstrated to be effective for the synthesis of perovskite materials (Huang et al., 1996; Y.; Li et al., 2010; Huízar-Félix et al., 2012). Moreover, the heat treatment at lower temperature (650°C) of the amorphous $AgNbO_3$ particles will avoid the reduction of silver. **Figure 2A,B** shows both $AgNbO_3$ and $Ag_{0.70}La_{0.10}{}^{\square}{}_{0.20}NbO_3$ agglomerated nanoparticles which are typical morphologies of sol-gel synthesis. $AgNbO_3$ particles are larger than those of $Ag_{0.70}La_{0.10}{}^{\square}{}_{0.20}NbO_3$, a feature confirmed by nitrogen adsorption measurements (BET method; **Supplementary Table S1**). These measurements revealed a specific surface area of $3\ m^2\ g^{-1}$ for $AgNbO_3$ and $13\ m^2\ g^{-1}$ for $Ag_{0.70}La_{0.10}{}^{\square}{}_{0.20}NbO_3$. In addition, as shown in **Supplementary Table S2**, EDX cationic ratio between Ag, La and Nb for every $Ag_{1-3x}La_x{}^{\square}{}_{2x}NbO_3$ confirms the presence of vacancies in all the powders of La-substituted $AgNbO_3$.

XRD was used to better understand the structural differences among all $Ag_{1-3x}La_x{}^{\square}{}_{2x}NbO_3$ powders. As shown in **Figure 3A.**, $AgNbO_3$ has a perovskite structure with no secondary phase, although splitting of several peaks is observed. $Ag_{0.85}La_{0.05}{}^{\square}{}_{0.10}NbO_3$ (x = 0.05) and $Ag_{0.70}La_{0.10}{}^{\square}{}_{0.20}NbO_3$ (x

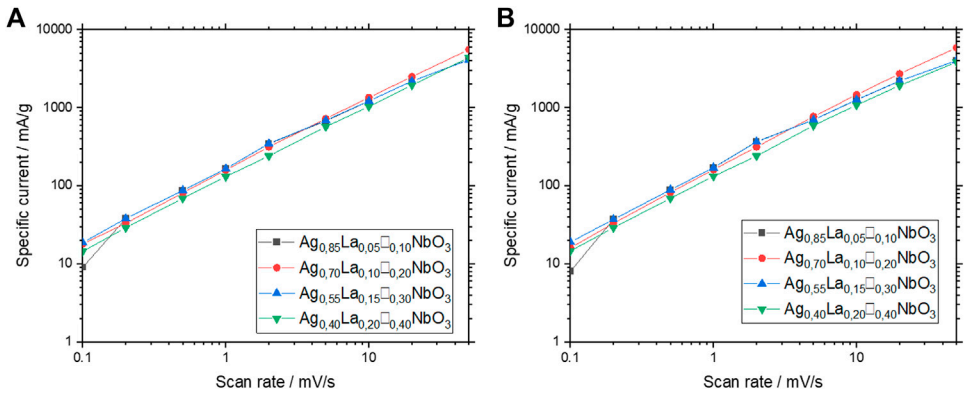

FIGURE 5 | (A) Linear regression from power law in the reduction peaks of $Ag_{1-3x}La_x\square_{2x}NbO_3$ for different value of x. **(B)** Linear regression from power law in the oxidation peaks of $Ag_{1-3x}La_x\square_{2x}NbO_3$ for different value of x.

TABLE 1 | *b* value of $Ag_{1-3x}La_x\square_{2x}NbO_3$ for different value of x for reduction and oxidation peaks.

	Reduction	Oxydation
$Ag_{0.85}La_{0.05}\square_{0.10}NbO_3$	0.94	0.95
$Ag_{0.70}La_{0.10}\square_{0.20}NbO_3$	0.92	0.95
$Ag_{0.55}La_{0.15}\square_{0.30}NbO_3$	0.87	0.87
$Ag_{0.40}La_{0.20}\square_{0.40}NbO_3$	0.9	0.91

= 0.10) also show the perovskite structure with no secondary phase visible in the diffractograms. However, starting from x = 0.15, impurity peaks appear, perhaps due to the lack of cations on the A-site, resulting in collapse of the structure. This is in agreement with previous reports on the A-site substitution in $AgNbO_3$ (Li et al., 2009; Juang et al., 2016). Depending on the size of the dopant cation, the perovskite structure can accept up to a certain amount of substitution, sometimes accompanied by the appearance of extra peaks which correspond to secondary phases. The decrease in peak intensity for $Ag_{0.55}La_{0.15}\square_{0.30}NbO_3$ and $Ag_{0.40}La_{0.20}\square_{0.40}NbO_3$, compared to other samples, is an indicator of the stress caused by the high proportion of La in the perovskite. For the substituted oxides, a decrease in peak splitting was observed with increasing lanthanum substitution (**Figures 3B–C**). Further, the disappearance of peak splitting by x = 0.15 suggests a higher degree of symmetry in the substituted materials due to lower [NbO_6] octahedra distortion.

To get greater insight into the structure of the synthesized materials, Le Bail structural refinements were performed for each composition. First, as indicated in **Supplementary Figure S1**, the refinement of $AgNbO_3$ confirms that the Pbcm space group well represents the structure of $AgNbO_3$. Cell parameters of $AgNbO_3$ were extracted from the refinement as shown in **Supplementary Figure S2** and **Supplementary Table S3**. We found that the cell parameters and the cell volume increase with increasing substitution of La for $Ag_{1-3x}La_x\square_{2x}NbO_3$, which is in agreement with a previous report (Li et al., 2009). Moreover, this is consistent with a decrease of NbO_6 octahedra distortions previously described above. Refinements using a higher symmetry space group (Pm3m) have been performed to

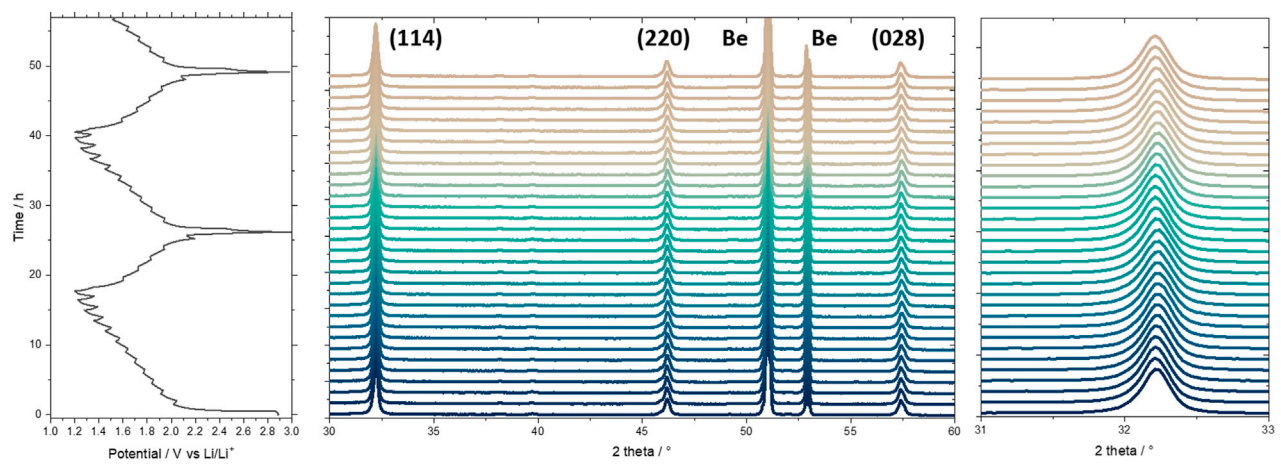

FIGURE 6 | *In situ* XRD patterns of the $Ag_{0.70}La_{0.10}\square_{0.20}NbO_3$ at a current of 0.02 A g^{-1} with corresponding voltage-time curve.

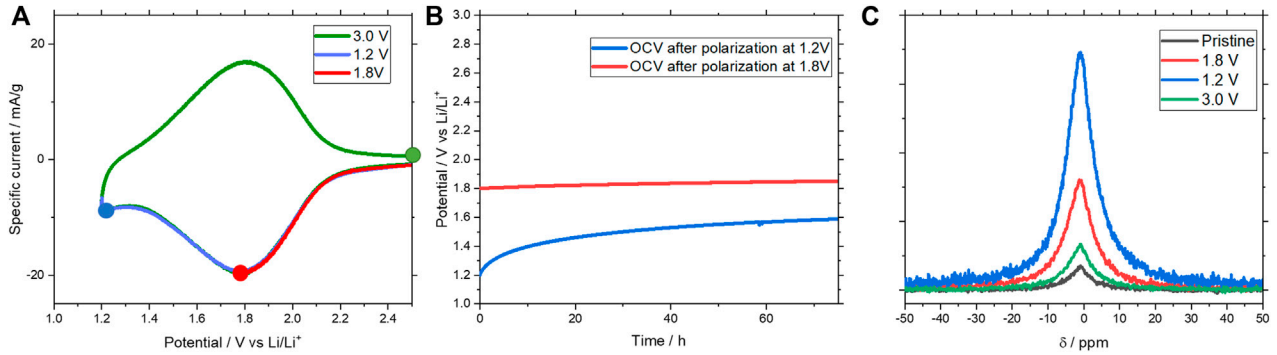

FIGURE 7 | (A) CV, **(B)** Self-discharge curves and **(C)** *ex situ* Li^7 MAS NMR normalized spectrum of the $Ag_{0.70}La_{0.10}\square_{0.20}NbO_3$ at different state of charge/discharge with associated CVs.

check that no phase transition appears with the substitution of silver by lanthanum. However, they did not lead to conclusive results. For this reason, we assume that the same space group (Pbcm) can be used to describe the crystallographic structure of all the $Ag_{1-3x}La_x\square_{2x}NbO_3$ powders.

To characterize the ability of this family of materials to reversibly store lithium ions, cyclic voltammetry at 0.1 mV s^{-1} was first performed. Note that this sweep rate should be considered as a low rate for power applications (around 5.5 h of charge). As depicted in **Figure 4A**, $AgNbO_3$ does not show any electrochemical activity between 1.2 and 3.0 V vs. Li^+/Li at the selected scan rate. A negligible specific capacity of 6 mAh.g^{-1} is reported. However, for each substituted material, broad and reversible peaks appear between 2.2 and 1.2 V vs. Li^+/Li, characteristic of lithium insertion into the host structure. Considering no insertion is visible for the unsubstituted oxide, we propose the following reaction **Eq. 2** to describe the present electrochemical reaction.

$$Ag_{1-3x}La_x\square_{2x}NbO_3 + yLi_x + ye^- \rightarrow Li_yAg_{1-3x}La_x\square_{2x}NbO_3 \quad (2)$$

At 0.1 mV s^{-1}, the specific capacity increases with the number of vacancies. During the first cycle at 0.1 mV s^{-1}, specific capacities are close to the theoretical capacity considering the insertion of one lithium ion per vacancy: 16 mAh g^{-1}, 35 mAh g^{-1}, 54 mAh g^{-1}, 76 mAh g^{-1} for $Ag_{0.85}La_{0.05}\square_{0.10}NbO_3$, $Ag_{0.70}La_{0.10}\square_{0.20}NbO_3$, $Ag_{0.55}La_{0.15}\square_{0.30}NbO_3$, $Ag_{0.40}La_{0.20}\square_{0.40}NbO_3$, respectively. Considering only the mass of active materials the gravimetric capacity is found to be equal to 38 mAh cm^{-3}, 109 mAh cm^{-3}, 206 mAh cm^{-3}, 219 mAh cm^{-3} and 264 mAh cm^{-3} for $AgNbO_3$, $Ag_{0.85}La_{0.05}\square_{0.10}NbO_3$, $Ag_{0.70}La_{0.10}\square_{0.20}NbO_3$, $Ag_{0.55}La_{0.15}\square_{0.30}NbO_3$, $Ag_{0.40}La_{0.20}\square_{0.40}NbO_3$, respectively. If the entire volume of the practical electrode is now considered (porosity volume ~70%), the gravimetric capacity is found to be equal to 12 mAh cm^{-3}, 32 mAh cm^{-3}, 62 mAh cm^{-3}, 66 mAh cm^{-3} and 79 mAh cm^{-3} for $AgNbO_3$, $Ag_{0.85}La_{0.05}\square_{0.10}NbO_3$, $Ag_{0.70}La_{0.10}\square_{0.20}NbO_3$, $Ag_{0.55}La_{0.15}\square_{0.30}NbO_3$, $Ag_{0.40}La_{0.20}\square_{0.40}NbO_3$, respectively. Interestingly, no reduction of silver is observed in these materials indicating the strong interaction of silver cations within the perovskite structure, contrary to most silver-based materials reported in the literature, i.e., silver vanadates (West and Crespi 1995; Marschilok et al., 2010; Sauvage et al., 2010).

Cyclic voltammetry was used to characterize the performance of the lanthanum-substituted oxides at a higher sweep rate of 2 mV s^{-1} (**Figure 4B**). This sweep rate corresponds to 15 min of charge/discharge, which is consistent with the current goal for the development of electric vehicles (Colclasure et al., 2019). As was observed at 0.1 mV s^{-1}, the CVs shown at 2 mV s^{-1} present very broad and reversible redox peaks.

As expected, the capacity of $AgNbO_3$ remains very low compared to the substituted oxides. Its capacity is 5 mA h.g^{-1}. $Ag_{0.85}La_{0.05}\square_{0.10}NbO_3$ is the least substituted material and the one with the lower capacity at both 0.1 mV s^{-1} and 2 mV s^{-1} (32 mAh g^{-1}). Interestingly, at 2 mV s^{-1}, $Ag_{0.40}La_{0.20}\square_{0.40}NbO_3$ has a lower capacity than $Ag_{0.70}La_{0.10}\square_{0.20}NbO_3$ and $Ag_{0.55}La_{0.15}\square_{0.30}NbO_3$, even though $Ag_{0.40}La_{0.20}\square_{0.40}NbO_3$ shows the higher theoretical capacity most likely attributed to the higher amount of vacancies per unit cell. Such a decrease in capacity is explained by the lower degree of crystallinity which does not allow adequate diffusion of lithium ions in this substituted oxide. Moreover, the defects detected by the presence of peaks that did not belong to the orthorhombic lattice provides another possible explanation to the lower capacity of $Ag_{0.40}La_{0.20}\square_{0.40}NbO_3$ at 2 mV s^{-1}. In addition, these CVs show the polarization between the oxidation and reduction peaks to be very small for each compound, even for CV at 2 mV s^{-1}. This result suggests that the intercalation process is not limited severely by low ionic diffusion, a consideration which will be discussed later.

CVs at different scan rates were performed to assess the capacity retention as a function of increasing scan rate. Scan rates from 0.1 mV s^{-1} to 50 mV s^{-1} were chosen, corresponding to 5.5h and 40s of charge, respectively. **Figures 4C,D** shows the specific capacity and relative capacity of every material at the mentioned scan rates. $Ag_{0.40}La_{0.20}\square_{0.40}NbO_3$, the material with the highest number of vacancies, provides the highest capacity at a low sweep rate (**Figure 4C**). However, when the scan rate is increased, a rapid decrease in capacity is observed starting at 0.2 mV s^{-1}. As shown in **Figure 4D**, at 50 mV s^{-1}, $Ag_{0.40}La_{0.20}\square_{0.40}NbO_3$ retains only 34% of the initial capacity

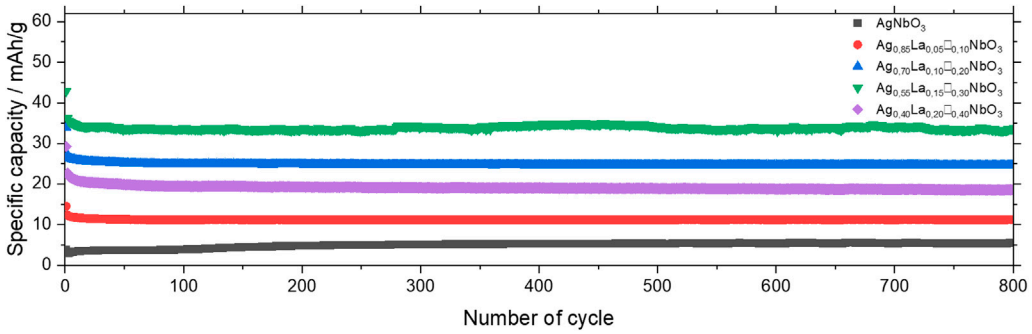

FIGURE 8 | Cycling stability of $Ag_{1-3x}La_x\square_{2x}NbO_3$ at 2 mV s^{-1}

measured at 0.1 mV s^{-1}. Similarly, $Ag_{0.55}La_{0.15}\square_{0.30}NbO_3$ demonstrates a relatively high capacity at low scan rates but a rapid drop at higher rates. In contrast, while less substituted materials such as $Ag_{0.85}La_{0.05}\square_{0.10}NbO_3$ and $Ag_{0.70}La_{0.10}\square_{0.20}NbO_3$ exhibit lower capacities at 0.1 mV s^{-1}, they demonstrate better capacity retention. At 50 mV s^{-1}, $Ag_{0.85}La_{0.05}\square_{0.10}NbO_3$, and $Ag_{0.70}La_{0.10}\square_{0.20}NbO_3$ exhibit capacity retentions of 53 and 64%, respectively, for a 500 times faster rate of charge/discharge compared to their capacities measured at 0.1 mV s^{-1}. All the specific capacities are summarized in **Supplementary Table S4**.

In order to get a better understanding of the charge storage mechanism, *b*-values from the power law relationship in **Eq. 3** have been calculated,

$$i = a.v^b \tag{3}$$

where i is the intensity of reduction/oxidation peak, v the corresponding scan rate, *a* and *b* are constant values. If *b* is close to 0.5, charge storage can be described as limited by ionic diffusion in the host material, as described in the Randles-Ševčík equation (Ševčík 1948; Randles 1948). When the value of *b* is equal or close to 1, charge storage occurs in agreement with non-diffusion limited mechanism, as in the case of pseudocapacitive materials (Choi et al., 2020). Regarding $Ag_{1-3x}La_x\square_{2x}NbO_3$ compounds, as shown in **Figure 5A,B**, a linear relationship between specific current and scan rate (0.1 mV s^{-1} and 50 mV s^{-1}) is observed, the *b*-values of which are listed in **Table 1**. The values of *b* vary between 0.87 and 0.95, which seems to indicate weak diffusion limitation during charge/discharge processes. Additionally, the smaller *b* values calculated for $Ag_{0.55}La_{0.15}\square_{0.30}NbO_3$ and $Ag_{0.40}La_{0.20}\square_{0.40}NbO_3$ support the difference in capacity retention observed previously, as compared to $Ag_{0.85}La_{0.05}\square_{0.10}NbO_3$, and $Ag_{0.70}La_{0.10}\square_{0.20}NbO_3$.

As displayed in **Figure 6**, the behavior of the different oxides during lithium insertion was investigated by *in situ* XRD, to better understand the filling of the vacant A-sites of the $Ag_{1-3x}La_x\square_{2x}NbO_3$ perovskite. $Ag_{0.70}La_{0.10}\square_{0.20}NbO_3$ was used because no structural defects were observed in this phase compared to $Ag_{0.55}La_{0.15}\square_{0.30}NbO_3$ and $Ag_{0.40}La_{0.20}\square_{0.40}NbO_3$. First, no new peak appears (and/or disappears) on the XRD patterns during charge and discharge. This behavior indicates that a solid solution type mechanism predominates upon charge storage, as previously reported for intercalation materials dedicated to power application with a *b* value close to 1 (Come et al., 2014). Moreover, it is observed that the peaks initially present do not move during lithiation. The three diffraction peaks observed in the studied 2θ range present the three crystallographic directions, implying that the perovskite structure does not modify its lattice parameters during lithium cation insertion in the vacant A sites. Thus, this material can be considered as a zero strain oxide during lithium insertion, similar to the well-known $Li_4Ti_5O_{12}$ (Thackeray and Amine 2021).

In another series of measurements, self-discharge and NMR experiments carried out on cycled $Ag_{0.70}La_{0.10}\square_{0.20}NbO_3$ electrodes provide further evidence of Li^+ insertion in the material. For these experiments, electrodes were cycled to 1.8 and 1.2 V vs. Li^+/Li at 0.1 mV s^{-1} and subsequently polarized for 10 h to reach a thermodynamic equilibrium. As shown in **Figure 7A,B**, both electrodes (cycled at 1.2 and 1.8 V vs. Li^+/Li) present relatively low self-discharge. The electrode polarized at 1.8V shows a potential of 1.82 V vs. Li^+/Li after almost 80 h of OCV. The electrode polarized at 1.2 V shows a potential of 1.59 V *vs.* Li^+/Li in the same condition. These low self-discharge levels at 1.2 and 1.8 V are a strong indication that lithium cations are inserted in a stable way into the vacancies of the material. *Ex situ* ^{7}Li MAS NMR measurements have been performed after these self-discharge experiments. ^{7}Li MAS NMR spectra were also recorded for the pristine and the fully discharged electrode (3.0V) in addition to the charged samples at 1.2 V vs. Li^+/Li, at a similar scan rate of 0.1 mV s^{-1}. As expected, the pristine electrode has a negligible quantity of Li detected. For the partially and fully charged samples, a peak is observed at around −1 ppm. The integrated intensity of the NMR peak, which is intrinsically proportional to the detected amount of lithium in the materials, is also found to be proportional to the specific capacity of the materials at 1.8 and 1.2 V (**Figure 7B,C**). The spectrum of the fully discharged electrode at 3.0V displays a small amount of lithium assigned to the partial irreversibility of the reaction during the first cycle and is also found to be in agreement with the first cycle of the CV. Due to the amount of lithium inserted in the materials, the signal to noise ratio remains relatively low even for a large

number of scans. For this reason, spectra with a narrower linewidth and thus better resolution, were not possible. Thus, it is difficult to conclude as to the number of lithium sites, even at the fully charged state, as only one apparent resonance is observed in ^{7}Li MAS NMR. Taken together, the combination of *ex situ* NMR and self-discharge provide convincing evidence that lithium ions are inserted in this perovskite material, most probably in the vacant A site.

The cycling characteristics for $Ag_{1-3x}La_x\square_{2x}NbO_3$ were determined as cycle life is a key property for the development of batteries based on high rate electrode materials. As observed in **Figure 8**, all the materials exhibit exceptional stability upon cycling. After 800 cycles at 2 mV s^{-1}, $Ag_{0.85}La_{0.05}\square_{0.10}NbO_3$, $Ag_{0.70}La_{0.10}\square_{0.20}NbO_3$, $Ag_{0.55}La_{0.15}\square_{0.30}NbO_3$ and $Ag_{0.40}La_{0.20}\square_{0.40}NbO_3$ show a capacity retention of 95, 95, 97 and 88%, respectively. The *in situ* XRD experiments and *b*-value calculation, which show zero-strain materials and non-diffusion limited charge storage mechanisms, respectively, are consistent with the outstanding cyclability observed for these materials.

In contrast to the classical design of insertion materials, our approach was to synthesize an oxide with vacancies in order to create potential sites for cation insertion in a perovskite. As proven by *ex situ* MAS NMR, lithium ions can be reversibly stored in the A site of $Ag_{0.70}La_{0.10}\square_{0.20}NbO_3$ and by extension to every $Ag_{1-3x}La_x\square_{2x}NbO_3$ composition. To further demonstrate this point, **Supplementary Figure S3A–D** presents the difference between lithium and sodium insertion by cyclic voltammetry at different scan rates. While Li^+ insertion leads to characteristic redox peaks, in the case of Na^+, no redox reaction can be observed. It is likely that sodium ions cannot be inserted into the structure of $Ag_{0.70}La_{0.10}\square_{0.20}NbO_3$ and therefore cannot generate redox reactions due to the larger ionic radius This is also the case for the pseudocapacitive T-Nb_2O_5, which shows highly reversible Li-ion intercalation but negligible Na-ion insertion (Kim et al., 2012). Moreover, kinetic analysis provides compelling evidence that a not diffusion-limited insertion occurs during the charge and discharge processes.

CONCLUSION

This work presents the partial substitution of $AgNbO_3$ perovskite by lanthanum in the A-site, resulting in the creation of cationic vacancies. We report on a gradual increase of the capacity at low scan rates as a function of the increase of the substitution. In addition, the different oxides present excellent behavior at high scan rates. At 50 mV.s^{-1} $Ag_{0.70}La_{0.10}\square_{0.20}NbO_3$ retains 64% of its capacity measured at 0.1 mV s^{-1}. Moreover, the combination of *ex situ* MAS NMR and *in situ* XRD experiments confirm that the insertion of lithium ions in the A site of the perovskite is responsible for the observed capacity and does not cause any structural change of the material. Together, these observations help to explain the good cycling behavior observed. In addition to structural insight, kinetic analysis indicates a non-diffusion limited ion insertion process for these oxides.

Nevertheless, some questions still remain. A better understanding of the solvation/desolvation occurring at the surface of particles during alkali ion insertion is critical towards understanding the small limitation of diffusion in charge storage process (Wang et al., 2019). Further experiments such as EQCM or *operando* atomic force microscopy can provide more insight in the charge storage mechanism. From another point of view, the promising observations reported here should be explored with other vacancy-designed materials and with different alkali cations. Moreover, these oxides present a charge storage mechanism which are between double layer capacitor and battery type electrodes (as observed for MnO_2 (Toupin et al., 2004; Brousse et al., 2006), T-Nb_2O_5 (Augustyn et al., 2013; Griffith et al., 2016) or MXenes (Naguib et al., 2012; Anasori et al., 2017) and represent an interesting model material for fundamental understanding in general.

In conclusion, the new approach reported in this work presents a different type of material design which widens the opportunities for creating the next generation of negative electrodes for high power Li- ion batteries. Although the oxide presented here contains silver, we believe this study can open the way toward the search of more practical materials for high-power battery electrodes.

DATA AVAILABILITY STATEMENT

The raw data supporting the conclusion of this article will be made available by the authors, without undue reservation.

AUTHOR CONTRIBUTIONS

ELC: Investigation, Methodology, Writing—review and editing. JCEA and ND: Investigation, Writing—review. BD and GW: Writing—review. OC and TB: Conceptualization, Methodology, Supervision, Writing—review and editing.

FUNDING

Nantes Université/NExT program (ANR-16-IDEX-0007, DISCUSS project).

ACKNOWLEDGMENTS

The authors want to thank University of Nantes and NExT program for financial funding. They also thank Eric Gautron for TEM/STEM images as well as Stéphane Grolleau for specific surface area measurement.

SUPPLEMENTARY MATERIAL

The Supplementary Material for this article can be found online at: https://www.frontiersin.org/articles/10.3389/fchem.2022.873783/full#supplementary-material

REFERENCES

Anasori, B., Lukatskaya, M. R., and Gogotsi, Y. (2017). 2D Metal Carbides and Nitrides (MXenes) for Energy Storage. *Nat. Rev. Mater.* 2 (2), 16098. doi:10.1038/natrevmats.2016.98

Armand, M., and Tarascon, J.-M. (2008). Building Better Batteries. *Nature* 451 (7179), 652–657. doi:10.1038/451652a

Augustyn, V., Come, J., Lowe, M. A., Kim, J. W., Taberna, P.-L., Tolbert, S. H., et al. (2013). High-rate Electrochemical Energy Storage through Li+ Intercalation Pseudocapacitance. *Nat. Mater* 12 (6), 518–522. doi:10.1038/nmat3601

Brousse, T., Toupin, M., Dugas, R., Athouël, L., Crosnier, O., and Bélanger, D. (2006). Crystalline MnO_2 as Possible Alternatives to Amorphous Compounds in Electrochemical Supercapacitors. *J. Electrochem. Soc.* 153 (12), A2171. doi:10.1149/1.2352197

Burnham, A., Dufek, E. J., Stephens, T., Francfort, J., Michelbacher, C., Carlson, R. B., et al. (2017). Enabling Fast Charging - Infrastructure and Economic Considerations. *J. Power Sourc.* 367 (novembre), 237–249. doi:10.1016/j.jpowsour.2017.06.079

Butts, D., Schoiber, J., Choi, C., Redhammer, G. J., Hüsing, N., Donne, S., et al. (2021). Fe-Substituted Sodium β''-Al_2O_3 as a High-Rate Na-Ion Electrode. *Chem. Mater.* 33 (15), 6136–6145. doi:10.1021/acs.chemmater.1c01680

Choi, C., Ashby, D. S., Butts, D. M., DeBlock, R. H., Wei, Q., Lau, J., et al. (2020). Achieving High Energy Density and High Power Density with Pseudocapacitive Materials. *Nat. Rev. Mater.* 5 (1), 5–19. doi:10.1038/s41578-019-0142-z

Chun, S., Grudinin, D., Lee, D., Kim, S.-H., Yi, G.-R., and Hwang, I. (2009). Roll-to-Roll Printing of Silver Oxide Pastes and Low Temperature Conversion to Silver Patterns. *Chem. Mater.* 21 (2), 343–350. doi:10.1021/cm802475m

Colclasure, A. M., Dunlop, A. R., Trask, S., Polzin, B. J., Jansen, A. N., and Smith, K. (2019). Requirements for Enabling Extreme Fast Charging of High Energy Density Li-Ion Cells while Avoiding Lithium Plating. *J. Electrochem. Soc.* 166 (8), A1412–A1424. doi:10.1149/2.0451908jes

Come, J., Augustyn, V., Kim, J. W., Rozier, P., Taberna, P.-L., Gogotsi, P., et al. (2014). Electrochemical Kinetics of Nanostructured Nb_2O_5 Electrodes. *J. Electrochem. Soc.* 161 (5), A718–A725. doi:10.1149/2.040405jes

Farid, U., Khan, H. U., Avdeev, M., Whittle, T. A., and Kennedy, B. J. (2019). Preparation and High Resolution Structural Studies of $Li_xAg_{1-x}NbO_3$ lead Free Piezoelectrics. *J. Solid State. Chem.* 269 (janvier), 401–408. doi:10.1016/j.jssc.2018.10.007

Gao, J., Liu, Q., Dong, J., Wang, X., Zhang, S., and Li, J.-F. (2020). Local Structure Heterogeneity in Sm-Doped $AgNbO_3$ for Improved Energy-Storage Performance. *ACS Appl. Mater. Inter.* 12 (5), 6097–6104. doi:10.1021/acsami.9b20803

Gao, J., Zhang, Y., Zhao, L., Lee, K.-Y., Liu, Q., Studer, A., et al. (2019). Enhanced Antiferroelectric Phase Stability in La-Doped $AgNbO_3$: Perspectives from the Microstructure to Energy Storage Properties. *J. Mater. Chem. A.* 7 (5), 2225–2232. doi:10.1039/C8TA09353A

Gogotsi, Y., and Simon, P. (2011). True Performance Metrics in Electrochemical Energy Storage. *Science* 334 (6058), 917–918. doi:10.1126/science.1213003

Griffith, K. J., Forse, A. C., Griffin, J. M., and Grey, C. P. (2016). High-Rate Intercalation without Nanostructuring in Metastable Nb_2O_5 Bronze Phases. *J. Am. Chem. Soc.* 138 (28), 8888–8899. doi:10.1021/jacs.6b04345

Griffith, K. J., Seymour, I. D., Hope, M. A., Butala, M. M., Lamontagne, L. K., Preefer, M. B., et al. (2019). Ionic and Electronic Conduction in $TiNb_2O_7$. *J. Am. Chem. Soc.* 141 (42), 16706–16725. doi:10.1021/jacs.9b06669

Griffith, K. J., Wiaderek, K. M., Cibin, G., Marbella, L. E., and Grey, C. P. (2018). Niobium Tungsten Oxides for High-Rate Lithium-Ion Energy Storage. *Nature* 559 (7715), 556–563. doi:10.1038/s41586-018-0347-0

Huang, K., Feng, M., and Goodenough, J. B. (1996). Sol-Gel Synthesis of a New Oxide-Ion Conductor Sr- and Mg-Doped $LaGaO_3$ Perovskite. *J. Am. Ceram. Soc.* 79 (4), 1100–1104. doi:10.1111/j.1151-2916.1996.tb08554.x

Huízar-Félix, A. M., Hernández, T., de la Parra, S., Ibarra, J., and Kharisov, B. (2012). Sol-gel Based Pechini Method Synthesis and Characterization of $Sm_{1-x}Ca_xFeO_3$ Perovskite $0.1 \leq x \leq 0.5$. *Powder Techn.* 229 (octobre), 290–293. doi:10.1016/j.powtec.2012.06.057

Juang, Y., Chu, S.-Y., and Wang, K. S. (2016). Phase Transition and Dielectric Properties of Sr-Doped $AgNbO_3$ Ceramics. *Ferroelectrics* 493 (1), 54–61. doi:10.1080/00150193.2016.1133216

Kim, J. W., Augustyn, V., and Dunn, B. (2012). The Effect of Crystallinity on the Rapid Pseudocapacitive Response of Nb_2O_5. *Adv. Energ. Mater.* 2 (1), 141–148. doi:10.1002/aenm.201100494

Leriche, J. B., Hamelet, S., Shu, J., Morcrette, M., Masquelier, C., Ouvrard, G., et al. (2010). An Electrochemical Cell for Operando Study of Lithium Batteries Using Synchrotron Radiation. *J. Electrochem. Soc.* 157 (5), A606. doi:10.1149/1.3355977

Li, G., Kako, T., Wang, D., Zou, Z., and Ye, J. (2009). Enhanced Photocatalytic Activity of La-Doped $AgNbO_3$ under Visible Light Irradiation. *Dalton Trans.* 0 (13), 2423–2427. doi:10.1039/B810126D

Li, M., Feng, M., Luo, D., and Chen, Z. (2020). Fast Charging Li-Ion Batteries for a New Era of Electric Vehicles. *Cel Rep. Phys. Sci.* 1 (10), 100212. doi:10.1016/j.xcrp.2020.100212

Li, Y., Yao, S., Wen, W., Xue, L., and Yan, Y. (2010). Sol-gel Combustion Synthesis and Visible-Light-Driven Photocatalytic Property of Perovskite $LaNiO_3$. *J. Alloys Comp.* 491 (1), 560–564. doi:10.1016/j.jallcom.2009.10.269

Marschilok, A. C., Kozarsky, E. S., Tanzil, K., Zhu, S., Takeuchi, K. J., and Takeuchi, E. S. (2010). Electrochemical Reduction of Silver Vanadium Phosphorous Oxide, $Ag_2VO_2PO_4$: Silver Metal Deposition and Associated Increase in Electrical Conductivity. *J. Power Sourc.* 195 (19), 6839–6846. doi:10.1016/j.jpowsour.2010.04.033

Massiot, D., Fayon, F., Capron, M., King, I., Le Calvé, S., Alonso, B., et al. (2002). Modelling One- and Two-Dimensional Solid-State NMR Spectra. *Magn. Reson. Chem.* 40 (1), 70–76. doi:10.1002/mrc.984

Naguib, M., Come, J., Dyatkin, B., Presser, V., Taberna, P.-L., Simon, P., et al. (2012). MXene: a Promising Transition Metal Carbide Anode for Lithium-Ion Batteries. *Electrochemistry Commun.* 16 (1), 61–64. doi:10.1016/j.elecom.2012.01.002

Prakash, A. S., Manikandan, P., Ramesha, K., Sathiya, M., Tarascon, J.-M., and Shukla, A. K. (2010). Solution-Combustion Synthesized Nanocrystalline $Li_4Ti_5O_{12}$ as High-Rate Performance Li-Ion Battery Anode. *Chem. Mater.* 22 (9), 2857–2863. doi:10.1021/cm100071z

Randles, J. E. B. (1948). A Cathode ray Polarograph. Part II.-The Current-Voltage Curves. *Trans. Faraday Soc.* 44 (0), 327–338. doi:10.1039/TF9484400327

Sauvage, F., Bodenez, V., Tarascon, J.-M., and Poeppelmeier, K. R. (2010). Room-Temperature Synthesis Leading to Nanocrystalline $Ag_2V_4O_{11}$. *J. Am. Chem. Soc.* 132 (19), 6778–6782. doi:10.1021/ja1009713

Sciau, P., Kania, A., Dkhil, B., Suard, E., and Ratuszna, A. (2004). Structural Investigation of $AgNbO_3$ Phases Using X-ray and Neutron Diffraction. *J. Phys. Condens. Matter* 16 (16), 2795–2810. doi:10.1088/0953-8984/16/16/004

Ševčík, A. (1948). Oscillographic Polarography with Periodical Triangular Voltage. *Collection Czechoslovak Chem. Commun.* 13, 349–377.

Shannon, R. D., and Prewitt, C. T. (1969). Effective Ionic Radii in Oxides and Fluorides. *Acta Crystallogr. Sect B* 25 (5), 925–946. doi:10.1107/S0567740869003220

Shannon, R. D. (1976). Revised Effective Ionic Radii and Systematic Studies of Interatomic Distances in Halides and Chalcogenides. *Acta Cryst. Sect A.* 32 (5), 751–767. doi:10.1107/S0567739476001551

Shin, D.-Y., Yi, G.-R., Lee, D., Park, J., Lee, Y.-B., Hwang, I., et al. (2013). Rapid Two-step Metallization through Physicochemical Conversion of Ag_2O for Printed "black" Transparent Conductive Films. *Nanoscale* 5 (11), 5043–5052. doi:10.1039/C3NR00962A

Sivakkumar, S. R., Nerkar, J. Y., and Pandolfo, A. G. (2010). Rate Capability of Graphite Materials as Negative Electrodes in Lithium-Ion Capacitors. *Electrochimica Acta* 55 (9), 3330–3335. doi:10.1016/j.electacta.2010.01.059

Song, K., Seo, D.-H., Jo, M. R., Kim, Y.-I., Kang, K., and Kang, Y.-M. (2014). Tailored Oxygen Framework of $Li_4Ti_5O_{12}$ Nanorods for High-Power Li Ion BatteryTailored Oxygen Framework of $Li_4Ti_5O_{12}$ Nanorods for High-Power Li Ion Battery. *J. Phys. Chem. Lett.* 5 (8), 1368–1373. doi:10.1021/jz5002924

Takeda, T., Takahashi, Y., Wada, N., and Sakabe, Y. (2003). Effects of Substitution of Na and K Ions for Ag Ion in $(Ag,Li)NbO_3$ Ceramics. *Jpn. J. Appl. Phys.* 42 (Part 1, No. 9B), 6023–6026. doi:10.1143/jjap.42.6023

Thackeray, M. M., and Amine, K. (2021). $Li_4Ti_5O_{12}$ Spinel Anodes. *Nat. Energ.* 6 (6), 683. doi:10.1038/s41560-021-00829-2

Toupin, M., Brousse, T., and Bélanger, D. (2004). Charge Storage Mechanism of MnO_2 Electrode Used in Aqueous Electrochemical Capacitor. *Chem. Mater.* 16 (16), 3184–3190. doi:10.1021/cm049649j

Valant, M., Axelsson, A.-K., Zou, B., and Alford, N. (2007). Oxygen Transport during Formation and Decomposition of $AgNbO_3$ and $AgTaO_3$. *J. Mater. Res.* 22 (6), 1650–1655. doi:10.1557/JMR.2007.0196

Wang, X., Mathis, T. S., Li, K., Lin, Z., Vlcek, L., Torita, T., et al. (2019). Influences from Solvents on Charge Storage in Titanium Carbide MXenes. *Nat. Energ.* 4 (3), 241–248. doi:10.1038/s41560-019-0339-9

West, K., and Crespi, A. M. (1995). Lithium Insertion into Silver Vanadium Oxide, $Ag_2V_4O_{11}$. *J. Power Sourc.* 54 (2), 334–337. doi:10.1016/0378-7753(94)02095-K

Wu, W., Liang, S., Chen, Y., Shen, L., Yuan, R., and Wu, L. (2013). Mechanism and Improvement of the Visible Light Photocatalysis of Organic Pollutants over Microcrystalline $AgNbO_3$ Prepared by a Sol-Gel Method. *Mater. Res. Bull.* 48 (4), 1618–1626. doi:10.1016/j.materresbull.2013.01.011

Conflict of Interest: The authors declare that the research was conducted in the absence of any commercial or financial relationships that could be construed as a potential conflict of interest.

Publisher's Note: All claims expressed in this article are solely those of the authors and do not necessarily represent those of their affiliated organizations, or those of the publisher, the editors and the reviewers. Any product that may be evaluated in this article, or claim that may be made by its manufacturer, is not guaranteed or endorsed by the publisher.